

Robustness versus sensitivity in non-Hermitian topological lattices probed by pseudospectra

Komis, Ioannis; Kaltsas, Dimitrios; Xia, Shiqi; Buljan, Hrvoje; Chen, Zhigang; Makris, Konstantinos G.

Source / Izvornik: **Physical Review Research, 2022, 4**

Journal article, Published version

Rad u časopisu, Objavljena verzija rada (izdavačev PDF)

<https://doi.org/10.1103/PhysRevResearch.4.043219>

Permanent link / Trajna poveznica: <https://urn.nsk.hr/urn:nbn:hr:217:259520>

Rights / Prava: [Attribution 4.0 International](#)/[Imenovanje 4.0 međunarodna](#)

Download date / Datum preuzimanja: **2025-03-27**







Repository / Repozitorij:

[Repository of the Faculty of Science - University of Zagreb](#)



Robustness versus sensitivity in non-Hermitian topological lattices probed by pseudospectra

Ioannis Komis ^{1,2}, Dimitrios Kaltsas ^{1,2}, Shiqi Xia,³ Hrvoje Buljan ^{3,4}, Zhigang Chen ^{3,5} and Konstantinos G. Makris ^{1,2}

¹*ITCP-Physics Department, University of Crete, Heraklion 71003, Greece*

²*Institute of Electronic Structure and Laser (IESL) FORTH, Heraklion 71110, Greece*

³*The MOE Key Laboratory of Weak-Light Nonlinear Photonics, TEDA Applied Physics Institute and School of Physics, Nankai University, Tianjin 300457, China*

⁴*Department of Physics, Faculty of Science, University of Zagreb, Bijenika c. 32, 10000 Zagreb, Croatia*

⁵*Department of Physics and Astronomy, San Francisco State University, California 94132, USA*



(Received 17 February 2022; accepted 13 September 2022; published 29 December 2022)

Non-Hermitian topological systems simultaneously possess two antagonistic features: ultrasensitivity due to exceptional points and robustness of topological zero-energy modes, and it is unclear which one prevails under different perturbations. We study that question by applying the pseudospectrum theory on the prototypical non-Hermitian Su-Schrieffer-Heeger lattice. Topological modes around the underlying third-order exceptional point (EP3) are robust with respect to chiral perturbations but sensitive to diagonal perturbations. In fact, exactly at the EP3 the chiral symmetry leads to a suppressed sensitivity, that corresponds to an EP2. Finally, for nonlinearly induced perturbations we provide a connection between the pseudospectrum approach and a nonlinear phase shift, which is relevant for experiments.

DOI: [10.1103/PhysRevResearch.4.043219](https://doi.org/10.1103/PhysRevResearch.4.043219)

I. INTRODUCTION

Non-Hermitian Hamiltonians in classical and quantum physics [1] describe the dynamics of open systems under the influence of dissipation and/or amplification. One of their intriguing characteristics is the existence of unique non-Hermitian degeneracies [2], the so-called exceptional points (EPs) [3], where two or more eigenvalues and eigenvectors coalesce for a particular value of the system's parameter [4,5], forming thus a higher-order exceptional point (HEP). Motivated by the recent introduction of the concept of parity-time (\mathcal{PT}) symmetry [6–8] in optics [9–13], where the spatial combination of gain and loss materials is physically accessible, the new area of non-Hermitian photonics [14–26] has emerged [27–31]. A plethora of experimental realizations of photonic devices that operate around the HEPs is evident, and is mainly based on the enhanced response of the system around such degeneracies. Among the most impressive experiments are these related to ultrasensitive sensors [25] and non-Hermitian gyroscopes [26].

On the other hand, topological photonics [32–38] relies on the key property of topological protection of the zero eigenstate. Especially in two dimensions, such an effect leads to the transport of optical waves along the edge of a photonic topological insulator, even under the presence of strong external perturbations. Most studies are so far devoted to Floquet sys-

tems with broken time-reversal symmetry that induce effective pseudomagnetic fields [34].

Recently, however, a new frontier that can be named as non-Hermitian topological photonics [39–43] has emerged, based on the synergy between the two aforementioned areas. This new direction has led to an explosion of theoretical and experimental results that exploit the existence of chiral and non-Hermitian symmetries on the same lattice. Among the recent experiments that define this field is the demonstration of \mathcal{PT} -symmetry breaking in a non-Hermitian Su-Schrieffer-Heeger (NHSSH) lattice [44,45], the topological insulator lasers [40,41], and the non-Hermitian Haldane lattice [43]. Nonlinearity also plays an important role and provides a new degree of freedom, as a relevant recent experiment demonstrated [46]. In fact, it allows us to locally control not only the real part of the index potential but the imaginary part as well. In such systems the inclusion of gain and loss elements makes the topological lattice non-Hermitian, and thus extends the physics of topological insulators to the complex domain, with no analog whatsoever in condensed matter physics. Since most of the previous concepts of topological physics have been built on the existence of conservation laws, based on Hermitian operators, it means that one has to derive everything from first principles by incorporating the intricate properties of non-Hermitian algebra. Indeed, Zak phases, Chern numbers, bulk-edge correspondence, and all relevant topological quantities must be redefined through the prism of non-Hermitian physics, leaving thus many open questions for further investigation [47–52].

In this context of non-Hermitian topological photonics, we examine the interplay between robustness (due to topology) and sensitivity (due to non-Hermiticity) in the prototypical system of an NHSSH lattice around the underlying HEPs [46].

Published by the American Physical Society under the terms of the Creative Commons Attribution 4.0 International license. Further distribution of this work must maintain attribution to the author(s) and the published article's title, journal citation, and DOI.

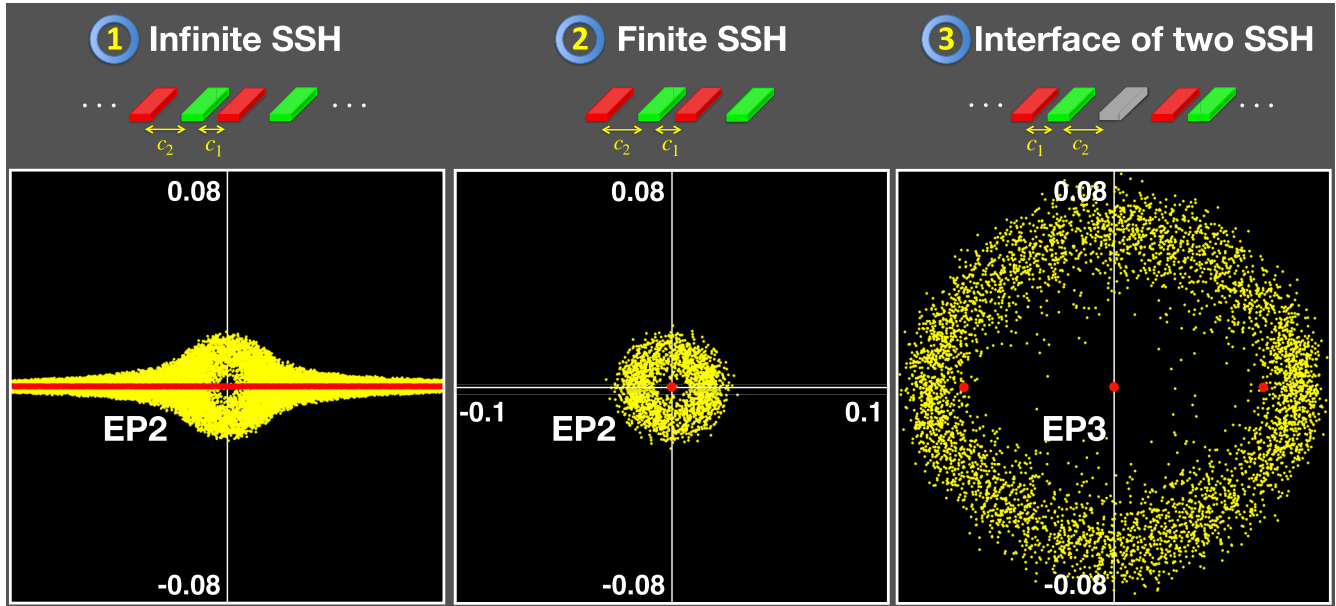


FIG. 1. Complex unstructured pseudospectra around the EPs of the three NHSSH lattices: infinite (left, $k \in [-\pi, -\pi + 0.08]$), finite (center, $N = 80$) for $\gamma = 2$, and interface (right, $N = 81$) for $\gamma = 2.0159$ and $\gamma_0 = 0$. In all cases $c_1 = 3$ and $c_2 = 1$. In the top row the red, green, and gray colors illustrate the gainy, lossy, and neutral waveguides, respectively. In the bottom row, the modes that form the EPs (conventional spectra, red dots) and corresponding 0.0001 pseudospectra (1000 realizations, yellow dots) for the three lattices are presented on the complex plane and on the same axes. We note here that in the interface lattice, at the red dot at $[0,0]$ three eigenvalues coalesce. We do not show the edge states of the finite SSH, which are located at $[0, \pm 2i]$ and the associated perturbations of the order $\varepsilon/2$.

In order to systematically examine the lattice sensitivity, we provide a mathematical framework ideal for non-Hermitian systems, that is, the complex and structured pseudospectra theory [53–56]. In particular, we consider three different lattices, namely, an infinite, a finite, and a heterostructure of two NHSSH lattices (see Fig. 1). The intricate relation between the lattice symmetry and the symmetries of the perturbations is revealed based on pseudospectra [53,54]. We find that for chiral structured perturbations, the topological zero state is indeed robust before the underlying EP n (the n th-order EP), as is physically expected. Furthermore, we find that exactly at EP3 the off-diagonal perturbations that respect chiral symmetry lead to a suppressed sensitivity that corresponds to an EP2. Counterintuitively, the zero states turn out to be most sensitive for unstructured complex perturbations, revealing the order of the pertinent exceptional point. At last we consider the lattices sensitivity due to single-site local perturbations of the interface channel; something that has been experimentally demonstrated using optical photorefractive nonlinearity [46].

II. NON-HERMITIAN SSH LATTICES

Our starting point is the prototypical SSH model, in the context of coupled mode theory. Under the paraxial approximation the wave evolution is governed by the coupled mode equations, which are

$$i \frac{\partial \psi_n}{\partial \xi} + \sum_m H_{n,m} \psi_m = 0, \quad (1)$$

where ξ is the propagation distance, ψ_n the complex amplitude of the field's envelope at the n th channel, and $H_{n,m}$ the real-space Hamiltonian elements. The corresponding right eigenvalue problem is $H|u_n^R\rangle = \lambda_n|u_n^R\rangle$, where the eigenvalues λ_n define the spectrum of the problem. The underlying symmetry of the lattices we examine here is $H^T = H$, which means that non-Hermiticity stems from the complex elements of Hamiltonian diagonal elements and not from any other asymmetry. Furthermore, the corresponding left eigenvalue problem of the adjoint matrix is $H^\dagger|u_n^L\rangle = \lambda_n^*|u_n^L\rangle$. We note here that the biorthogonality condition is $\langle u_m^L|u_n^R\rangle = \delta_{n,m}$ (where $\delta_{n,m}$ is the Kronecker delta) and since $H^\dagger = H^*$, the left and right eigenfunctions are complex conjugate pairs. In other words our matrix is symmetric. In general the spectrum of such lattices is complex, unless they respect the \mathcal{PT} symmetry. In this latter case, they may exhibit an entirely real spectrum.

More specifically, the lattices that we consider are schematically depicted in Fig. 1. For the infinite lattice, the Hamiltonian in k space reads

$$H^{\text{inf}}(k) = (c_2 + c_1 \cos k)\sigma_x + c_1 \sin k \sigma_y - i\gamma \sigma_z, \quad (2)$$

where $\sigma_x, \sigma_y, \sigma_z$ are the Pauli matrices and k is the Bloch wavenumber in the first Brillouin zone. The coupling constants are denoted by c_1 and c_2 for intra- and intercell coupling, respectively. The global gain-loss amplitude of each waveguide channel is described by the parameter γ , and thus making the whole system non-Hermitian. For the finite lattice the Hamiltonian matrix elements are

$$H_{nm}^{\text{fin}} = \delta_{n+1,m} c_{(n \bmod 2)+1} + \delta_{n,m+1} c_{(m \bmod 2)+1} + \delta_{nm} i\gamma_n, \quad (3)$$

where $\gamma_n = (-1)^n \gamma$, and $n, m = 1, \dots, N$ (see Appendix A). Regarding the last case of an interface SSH lattice, we consider two SSH chains that are connected with an extra channel at the interface that has a tunable gain-loss amplitude γ_0 . In such a case the Hamiltonian matrix elements are given in the Appendix B.

In all the three cases above, the associated matrices are non-Hermitian and symmetric, meaning $H^T = H$, unlike the Hatano-Nelson problems [57]. Thus their eigenvalue spectrum ($\{\lambda_n\}$) is in general complex. Depending on the value of the global gain-loss amplitude γ , we find that the first two lattices exhibit an EP2 and the interface lattice an EP3 (see Appendices A and B).

III. COMPLEX UNSTRUCTURED PSEUDOSPECTRA

In the vast majority of previous studies, the sensitivity of a non-Hermitian system under external perturbations was analyzed using the semianalytical techniques based on perturbation theory, for systems of usually small number of waveguides. For lattices of our type such an approach is rather problematic and is not easily applicable, since we do have to use different versions of perturbation theory depending how close we are at the underlying EPs, and with very limited types of perturbation strengths. Therefore we introduce an alternative and general computational framework based on *pseudospectra* [53]. The so-called pseudospectrum is a systematic mathematical way to study the sensitivity of a matrix/operator on external perturbations, without relying on perturbation theory. It has been extensively used in the context of fluid mechanics [54–56], non-normal networks [58], and transient growth physics [59–62]. However, it is largely unknown in optics despite being ideal for studying non-Hermitian systems [63–69]. For Hermitian matrices, the spectrum and the pseudospectrum are almost identical, whereas for non-Hermitian matrices they could be significantly different. The measure of how different the two spectra might be, depends on the degree of the nonorthogonality of the corresponding eigenmodes. Thus the pseudospectrum of a non-normal matrix provides us with complete information, beyond the conventional spectrum. The most basic definition of the ε pseudospectrum of a non-Hermitian matrix H , with a $\sigma(H)$ spectrum, is the union of all spectra of the matrices $H + E$, where E is a full complex random matrix (with respect to its matrix elements), with $\|E\| < \varepsilon$, where $\|\cdot\|$ is the matrix norm which is defined by $\|A\| = \sup_{x \neq 0} \frac{\|Ax\|}{\|x\|}$ [53]. More specifically, $\sigma_\varepsilon(H)$ is the set of $z \in \mathbb{C}$ such that $z \in \sigma(H + E)$ for some $E \in \mathbb{C}^{N \times N}$ with $\|E\| < \varepsilon$. Equivalently we have

$$\sigma_\varepsilon(H) \equiv \bigcup_{j=1, \|E_j\| < \varepsilon}^s \sigma(H + E_j), \quad (4)$$

where s is the number of different realizations of the perturbations. In particular,

$$E = \varepsilon \frac{E}{\|E\|}, \quad (5)$$

where ε defines the perturbation strength and the matrix E is the perturbation matrix before the normalization.

Our results for the three NHSSH lattices, are shown in Fig. 1 for gain-loss amplitude almost at the HEP. The red dots represent the spectrum and the yellow dots the corresponding pseudospectra. As we can see, the corresponding pseudospectra are extended patterns on the complex plane, and their size is related to the sensitivity of the lattice. In particular, the eigenstates close to the gap closing point are most sensitive and those away from that gap are more robust. From the complex eigenvalue bifurcation curves vs γ (see Appendices A and B), we can identify the modes that coalesce and form the HEPs. The geometrical size of the main lobe of the complex pseudospectrum as a function of the perturbation strength ε , has a square-root and cubic-root dependence, that are characteristic signatures of the EP2 and EP3, respectively, for small values of the perturbation strengths. Apart from characterizing sensitivity, the geometrical characteristics of the pseudospectrum can also provide information about the power growth dynamics in the case of a dissipative spectrum (when an overall gauge loss shift is applied to the whole lattice) [64]. As such, we want to find order of magnitude estimates for the power growth in order to characterize our systems. By applying the Kreiss matrix theorem of functional analysis of non-normal operators an upper and lower bound of $\mathcal{K}(\hat{M}) \leq \sup_{z \geq 0} \|e^{z\hat{M}}\| \leq eN\mathcal{K}(\hat{M})$ can be estimated, where e is the Euler's number, and the Kreiss-constant \mathcal{K} of the matrix $\hat{M} = i\hat{H}$ is defined as $\mathcal{K}(\hat{M}) \equiv \sup_{\text{Re}z > 0} \{\text{Re}z \|z\hat{I} - \hat{M}\|^{-1}\}$. For a global shift of loss (≈ 0.05), the Kreiss constant is $\mathcal{K}(\hat{M}) \approx 233$.

IV. STRUCTURED PSEUDOSPECTRA

Since the applied perturbations are complex and applied everywhere, even in the zero entries of the H matrix, we need to examine more realistic and experimentally relevant perturbations. Such perturbations are called structured perturbations and they define the *structured pseudospectrum* [53], which is ideal for studying the sensitivity of our NHSSH lattice. We define the structured pseudospectrum $\sigma_\varepsilon^{\text{str}}$ of the Hamiltonian H , as

$$\sigma_\varepsilon^{\text{str}}(H) \equiv \bigcup_{j=1, E\text{-structured}, \|E_j\| < \varepsilon}^s \sigma(H + E_j), \quad (6)$$

where s is the number of different realizations of the structured perturbations. The main difference from the unstructured (full) pseudospectra is that the matrix E is not full but has a particular structure that stems from the physics of the problem. For example, if the external perturbations are applied only on the index modulation (on site potential strength), then E is diagonal. If they are applied to the coupling coefficients (perturbing the distances between channels), then the ± 1 diagonals are nonzero. In other words, all the perturbations (real or complex) that we consider are physically relevant and experimentally realizable, since they are connected to perturbations of actual quantities of the lattice, namely, interchannel distance and on-site potential strength. One can consider various different combinations of perturbations for our three lattices (see Appendix C). But we focus our attention on diagonal ($E_{nm} = \delta_{n,m} z_n$) and off-diagonal (see Appendices) perturbations on the interface lattice. The real and the imaginary parts of the complex numbers z_n are drawn from the

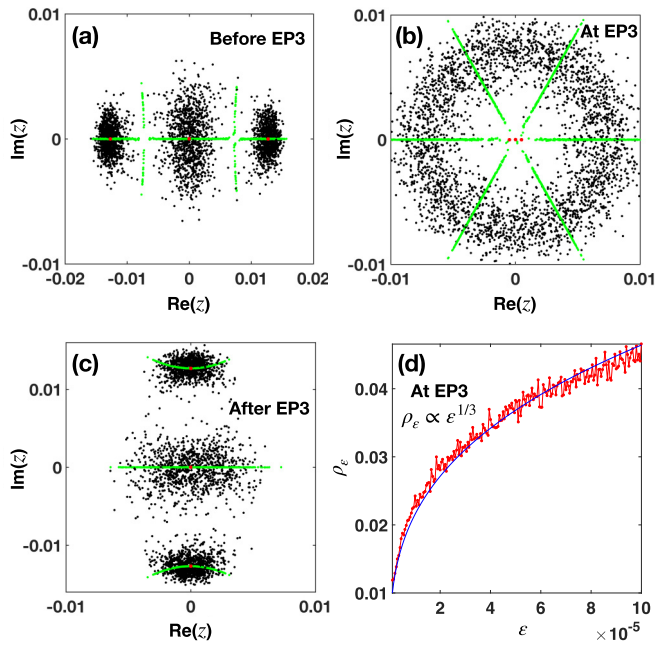


FIG. 2. (a)–(c) Structured diagonal pseudospectra $\sigma_{10^{-6}}^{\text{str}}(H)$ of the interface NHSSH lattice for the three eigenmodes that form the EP3, before ($\gamma = \gamma_{\text{EP3}} - 5 \times 10^{-5}$), at ($\gamma = \gamma_{\text{EP3}}$), and after ($\gamma = \gamma_{\text{EP3}} + 5 \times 10^{-5}$) the EP3, respectively, for $\gamma_{\text{EP3}} = 2.0159293$. We also include diagonal complex (black dots) and real (green dots) perturbations for $s = 1000$ realizations, and we do not see a significant difference. (d) Pseudospectral radius (red line) of (b) as a function of ε . The blue line is $\approx \varepsilon^{1/3}$ fit, shown for comparison.

normal distribution around zero, and their magnitudes are of the order of one. What is important though, is the value of ε that determines the physical strength of the applied perturbations due to Eq. (5).

Let us now examine the effect of diagonal perturbations on the interface lattice (Fig. 2), by calculating the corresponding structured pseudospectra before [Fig. 2(a)], at [Fig. 2(b)], and after the EP3 [Fig. 2(c)] on the complex plane. One characteristic signature of an EP3 is its extreme sensitivity, which we can clearly see in Fig. 2(c). Moreover, the size of the pseudospectrum can be quantitatively described by the pseudospectral radius ρ_ε [53], which is defined here locally as $\rho_\varepsilon \equiv \max_{z \in B} |z|$, with the z belonging on the subset $B \subset \sigma_\varepsilon(H)$ of interest. In Fig. 2(d) we calculate the pseudospectral radius of the central cloud at the gap ρ_ε of Fig. 2(c) for different values of ε . Such a radius is of the order of $\varepsilon^{1/3}$, as is known from the Lidskii perturbation theory of Jordan matrices, for very small perturbation strength [70]. Under this type of perturbations it is clear that the non-Hermitian sensitivity determines the behavior of our lattice close to EP3.

Let us now continue with off-diagonal perturbations (Fig. 3), by calculating the corresponding structured pseudospectra before [Fig. 3(a)], at [Fig. 3(b)], and after the EP3 [Fig. 3(c)] on the complex plane. Since they respect the chiral symmetry of the lattice, we expect the zero mode to be robust to such external perturbations for open gap, but what would happen exactly at EP3 for zero gap is a highly nontrivial problem. As we can see at Fig. 3(b) the pseudospectrum is

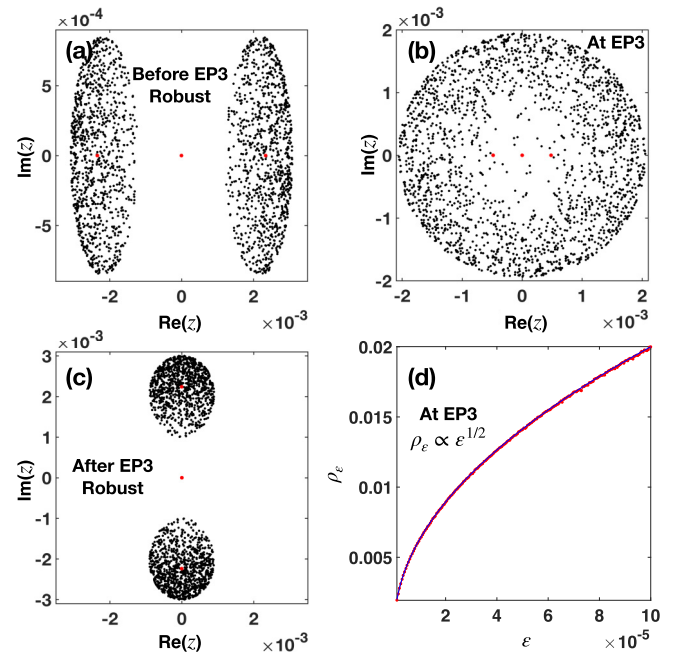


FIG. 3. (a)–(c) Structured off-diagonal pseudospectra $\sigma_{10^{-6}}^{\text{str}}(H)$ of the interface NHSSH lattice for the three eigenmodes that form the EP3, before ($\gamma = \gamma_{\text{EP3}} - 1.3 \times 10^{-6}$), at ($\gamma = \gamma_{\text{EP3}}$), and after ($\gamma = \gamma_{\text{EP3}} + 1.3 \times 10^{-6}$) the EP3, respectively. In comparison to Fig. 2(b) the sensitivity corresponds to an EP2. Therefore the chiral perturbations reduce the sensitivity of the EP. (d) Pseudospectral radius (red line) of (b) as a function of ε . The blue line is $\approx \varepsilon^{1/2}$ shown for comparison.

quite different than that of Fig. 2(b) for the same value of ε . Even more interestingly, from Fig. 3(d), we deduce that the corresponding sensitivity is that of an EP2. Thus we arrive at the striking and unexpected conclusion that even though the spectrum is the same in both cases, the pseudospectrum is not and reveals information about the reduced sensitivity of the system. Such reduction of the order of EP in terms of its sensitivity affects the sensitivity of other supermodes, as is evident from Figs. 3(a) and 3(c).

V. NONLINEARITY-INDUCED PERTURBATIONS

Until now we have examined structured or unstructured perturbations that are globally applied on the whole lattice, where the gain-loss amplitude of the interface channel γ_0 is equal to zero. It has been recently demonstrated experimentally [46], that by using the photorefractive nonlinear effect, we can control not only the real but also the imaginary value of the potential strength of the interface channel, namely $H_{(N-1)/2+1, (N-1)/2+1} = x_0 + i\gamma_0 = z_0$. Therefore, by tuning the nonlinearity we can effectively induce two different lattices: a lossy lattice if the interface channel is lossy ($\gamma_0 > 0$), and a gainy lattice when the interface channel is gainy ($\gamma_0 < 0$) (see Appendix F). Now we are interested to obtain the structured pseudospectra under nonlinearity-induced perturbations for chiral off-diagonal and real perturbations (Fig. 4). We find that the topological robustness of the zero mode is conserved, if and only if, our system has zero gain-loss

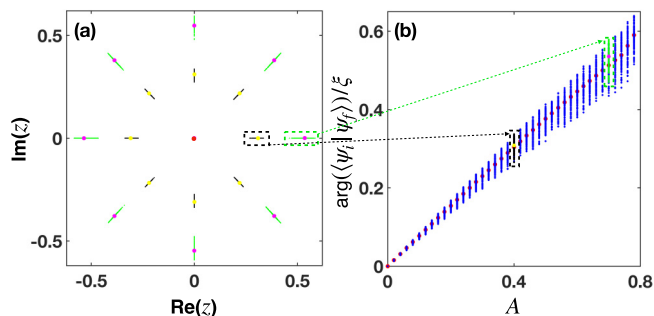


FIG. 4. Topological robustness and non-Hermitian sensitivity for chiral perturbations. (a) We vary locally the interface channel's potential strength for $\gamma = 1$. Magenta dots correspond to $|z_0| = 0.7$, while yellow dots correspond to $|z_0| = 0.4$. Green and black dots denote the corresponding eigenvalue fluctuations for 200 realizations of added perturbations of strength $\varepsilon = 20\%$. (b) Dynamical computation of nonlinear phase shift of the zero mode, for different strengths of nonlinearity A . The agreement with (a) is excellent.

amplitude at the interface channel, $\gamma_0 = 0$ [Fig. 4(a)]. Notice the robustness of the zero mode is also gradually lost as we move away from the value zero. Surprisingly, the change in the eigenvalue seems to have a preferred radial direction in the complex plane. From the experimental point of view, one could argue how to measure such a response based on the setup of [46]. In Fig. 4(b) we calculate the response of the zero mode under actual dynamics, under the action of cubic nonlinearity in the interface channel.

The dynamics is governed by the relation

$$i \frac{\partial \psi_n}{\partial \xi} + \sum_m H_{n,m} \psi_m + A \delta_{n,d} |\psi_d|^2 \psi_d = 0, \quad (7)$$

where A is the nonlinearity strength and ψ_d denotes the field amplitude at the defect channel. We find that the sensitivity of the zero mode is imprinted in the nonlinear phase due to the self-phase modulation effect. We calculate it as the angle between the input normalized zero mode ψ_i and the resulting final one ψ_f after some distance ξ , for each value of A . In other words, the pseudospectrum approach and the full dynamics converge for relative weak values of nonlinearity, and such a connection provides a direct link to our whole approach to measurable quantities. For higher values of the nonlinearity coefficient A the agreement becomes less apparent as expected.

VI. DISCUSSION AND CONCLUSIONS

As a general conclusion, non-Hermiticity has an immediate impact on a lattice's sensitivity rather than its topological structure. More specifically, we studied the effect of symmetries of the applied perturbations on the overall sensitivity in NHSSH lattices in terms of pseudospectra. In particular, for the interface lattice, the complex-unstructured and diagonal-structured pseudospectra describe the enhanced sensitivity (algebraic root dependence) before the EP3 and the chiral structured perturbations uncover the topological protection of the zero mode. Exactly at the EP3 (zero gap) the situation is more complex. In fact, chiral perturbations lead to reduction

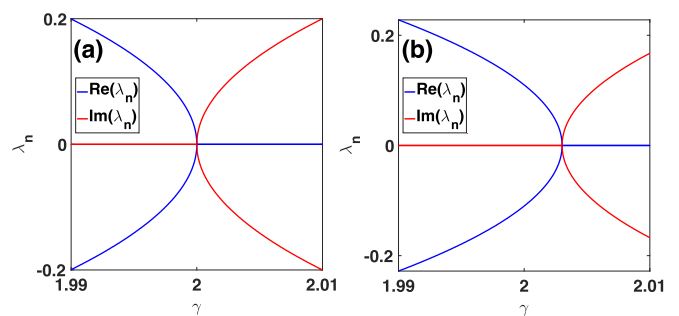


FIG. 5. (a),(b) Real (blue lines) and imaginary (red lines) parts of bifurcation eigenvalue curves vs the gain-loss amplitude of the infinite (for $k = -\pi$) and finite lattice, respectively. We only show the curves for the modes that form the EP2.

of the apparent sensitivity of the EP3 by one order (EP3 to EP2). Finally, we have examined the nonlinearly controlled pseudospectrum of the zero mode, spectrally and dynamically, where sensitivity and memory of the topological robustness coexist. Our results highlight the fundamental question of the interplay between ultrasensitivity and topological protection in the unique framework of pseudospectrum theory and may provide insight for the study of other lattices of non-Hermitian topological physics.

ACKNOWLEDGMENTS

This research is supported by the National Key R&D Program of China under Grant No. 2022YFA1404800 and the National Natural Science Foundation (12134006) in China. H.B. acknowledges support by the QuantiXLie Center of Excellence, a project cofinanced by the Croatian Government and European Union through the European Regional Development Fund—the Competitiveness and Cohesion Operational Programme (Grant No. KK.01.1.1.01.0004). This research was also supported in the frame of support for research activities, matching funds ($\Pi\Delta 00761$) by the IESL-FORTH.

APPENDIX A: SPECTRAL BIFURCATION CURVES OF INFINITE AND FINITE LATTICES

We demonstrate the existence of a second-order EP in the finite and infinite lattices. We plot the bifurcation curves of the real and imaginary parts of the eigenvalues of each lattice versus its gain-loss amplitude γ . The matrix Hamiltonians for the infinite and finite lattices are

$$H^{\text{inf}} = \begin{bmatrix} -i\gamma & c_2 + c_1 e^{-ik} \\ c_2 + c_1 e^{ik} & i\gamma \end{bmatrix}, \quad (A1)$$

$$H^{\text{fin}} = \begin{bmatrix} -i\gamma & c_2 & 0 & 0 & \dots \\ c_2 & i\gamma & c_1 & 0 & \dots \\ 0 & c_1 & -i\gamma & c_2 & \dots \\ 0 & 0 & c_2 & i\gamma & \dots \\ \vdots & \vdots & \vdots & \vdots & \ddots \end{bmatrix}, \quad (A2)$$

respectively.

Our results are shown in Fig. 5. In particular, Fig. 5(a) corresponds to the bifurcation eigenvalue curves for the infinite lattice that is described by the 2×2 Bloch Hamiltonian, while

Fig. 5(b) for the finite lattice of $N = 100$ waveguides. The coupling constants are $c_1 = 3$ and $c_2 = 1$. We plot the real (blue line) and imaginary (red line) parts of the eigenvalues that form the EP. As we can see, the two systems exhibit an EP2 at $\gamma = 2$. For the finite lattice it is closer to $\gamma \approx 2.004$ since we only have 100 channels. Increasing the number of channels leads to a value closer to two.

APPENDIX B: SPECTRAL BIFURCATION CURVES OF INTERFACE LATTICE

Now we study the spectrum of interface lattice, which consists of two SSH chains and one interface channel. We assume coupling constants $c_1 = 3$ and $c_2 = 1$ and 40 sites for each SSH chain, i.e., 81 sites total. The gain-loss amplitude of the lattice is $\gamma = 1$ while, for the interface channel it is $\gamma_0 = 0$. With these parameters we calculate the eigenmodes and eigenvalues (λ_n) of the matrix Hamiltonian which is given by the relation $H^{\text{int}} =$

$$\begin{bmatrix} -i\gamma & c_1 & 0 & 0 & \dots & \dots & \dots & \dots & \dots & \dots & 0 \\ c_1 & i\gamma & c_2 & 0 & \dots & \dots & \dots & \dots & \dots & \dots & 0 \\ 0 & c_2 & -i\gamma & c_1 & \dots & \dots & \dots & \dots & \dots & \dots & 0 \\ \vdots & \vdots & \vdots & \vdots & \ddots & \vdots & \vdots & \vdots & \vdots & \vdots & \vdots \\ 0 & \dots & \dots & c_1 & i\gamma & c_2 & \dots & \dots & \dots & \dots & 0 \\ 0 & \dots & \dots & \dots & c_2 & i\gamma_0 & c_2 & \dots & \dots & \dots & 0 \\ 0 & \dots & \dots & \dots & \dots & c_2 & -i\gamma & c_1 & \dots & \dots & 0 \\ \vdots & \vdots & \vdots & \vdots & \vdots & \vdots & \vdots & \vdots & \ddots & \vdots & \vdots \\ \vdots & \vdots & \vdots & \vdots & \vdots & \vdots & \vdots & \vdots & \vdots & \ddots & \vdots \\ \vdots & \vdots & \vdots & \vdots & \vdots & \vdots & \vdots & c_1 & i\gamma & c_2 & 0 \\ \vdots & \vdots & \vdots & \vdots & \vdots & \vdots & \vdots & \vdots & 0 & c_2 & -i\gamma & c_1 \\ 0 & \dots & \dots & \dots & \dots & \dots & \dots & 0 & 0 & c_1 & i\gamma \end{bmatrix}. \quad (\text{B1})$$

In Fig. 6(a) we show the eigenvalues in the complex plane. The red dots represent the five modes that form the first EPs of our system. These five modes coalesce in different ways, as we change γ and form the first EPs. The one in the middle, i.e., $\text{Re}(\lambda) = \text{Im}(\lambda) = 0$, is the defect mode. Since we know which modes form the EPs, we plot the corresponding bifurcation eigenvalue curves, which show how the system behaves as a function of a bifurcation parameter (global gain-loss amplitude here). Hence, if we plot the eigenvalues of the eigenmodes versus the gain-loss of the system we can find if there is any preferred point that all the curves meet. In general there can be many such points or even none.

In Fig. 6(b) we plot the real part (blue lines) and the imaginary part (red lines) of the eigenvalues as a function of the gain-loss amplitude of the system while keeping the gain-loss of the interface channel fixed. Notice that there are two EPs very close to each other for a gain-loss amplitude at around 2.015. Both of the EPs are of order three. The exact value for the first third-order EP is at $\gamma_{\text{EP3}} = 2.0159293$. For this one, we also plot the difference of the corresponding mode profiles. Figure 6(c) shows the difference between the absolute value of their amplitudes as pairs of two. Since there are three eigenmodes and the corresponding eigenvalues that coalesce, this is indeed a third-order EP. We refer to the n th element $u_{d,n}$ of the defect mode $|u_d\rangle$ and compare it with its neighboring modes.

Another criterion we use to determine the EP3 is to calculate the cosine of the angle between the corresponding modes that participate in the creation of the EP3, add them, and then

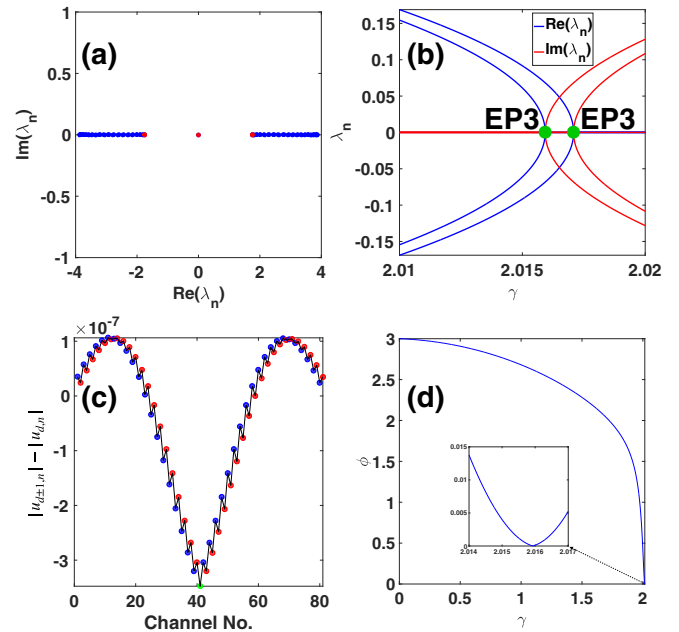


FIG. 6. (a) Spectrum of interface lattice for $\gamma_0 = 0$ in the complex plane. Red dots are the five modes for which we plot the bifurcation curves. (b) Real (blue lines) and imaginary (red lines) parts of bifurcation eigenvalue curves vs the gain-loss amplitude of the lattice, only for the red dots of (a). Green dots represent the EPs. (c) The difference between the three modes at the first EP3 as pairs of two. (d) The quantity ϕ as a function of the gain-loss amplitude of the lattice. Inset depicts a magnified view around the first EP3, and as we can see, $\phi = 0$.

subtract them from three. We define this quantity ϕ as

$$\phi = 3 - (\cos \theta_{d,d+1} + \cos \theta_{d,d-1} + \cos \theta_{d+1,d-1}), \quad (\text{B2})$$

where $\cos(\theta_{i,j}) = \frac{|u_i \cdot u_j|}{\|u_i\| \|u_j\|}$ with $|u_i\rangle$ being the eigenvectors of H . We expect in the Hermitian case, i.e., $\gamma = 0$, ϕ to be equal to three while, if there is an EP3, ϕ must be equal to zero since the modes are parallel and equal to each other. In Fig. 6(d) we plot the quantity ϕ as a function of gain-loss amplitude and in the inset we can see that indeed it is zero at the expected value.

APPENDIX C: DEFINITIONS OF PSEUDOSPECTRUM

The pseudospectrum of a system can either be structured or unstructured as we mentioned in the main text. We have also explained the advantages and disadvantages of each one. In this section we present the three different definitions of unstructured (complex) pseudospectrum that we used to compute our results, and in order to further demonstrate the efficiency of our method we compare them. It is crucial to remember that unstructured/full and complex pseudospectrum refer to the exact same definition.

If the norm of the operator is the Euclidean norm, which is always the case for the system that we examine here, the definition we mentioned in the main text is equivalent to the following one. The ε pseudospectrum is the set of $z \in \mathbb{C}$ such that $s_{\min}(zI - H) \leq \varepsilon$, where s_{\min} denotes the minimum singular value, computed via singular value decomposition

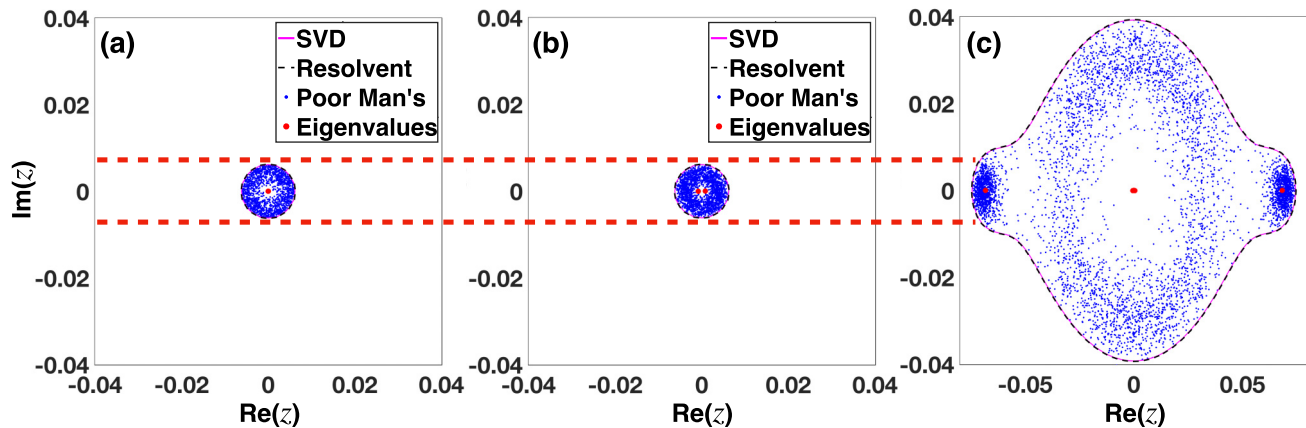


FIG. 7. Comparison of the different definitions of pseudospectra for a perturbation $\varepsilon = 10^{-5}$. As we expect, they are equivalent. In each plot the magenta line is the SVD method, the black dashed line the definition that uses the resolvent of the matrix, and the blue dots the “poor man’s” pseudospectrum. Finally, the red dots represent the eigenvalues of each lattice. (a) Comparison for the infinite lattice, where we consider only one Bloch momentum $k = -\pi$, at the EP. (b) Same for the finite lattice. Notice that the sizes are the same with (a) since both lattices exhibit an EP2. (c) Comparison of the methods for the interface lattice. At the center there are three different eigenvalues that coalesce. As we can see, for such a perturbation only the poor man’s method distinguishes the five eigenvalues close to zero. We compare the sensitivity due to the order of the EPs by comparing the size between the clouds of these three eigenvalues and the eigenvalues of the other two lattices (red dashed lines).

(SVD) of the matrix $zI - H$ for every different number z in the complex plane. It describes how an external perturbation affects our system without performing perturbation theory. This definition is given in mathematical terms by the following relation, where $\sigma(H)$ denotes the eigenvalue spectrum of the Hamiltonian,

$$\sigma_\varepsilon(H) = \{z \in \mathbb{C} : s_{\min}(zI - H) \leq \varepsilon\}, \quad (\text{C1})$$

and equivalently using the resolvent of the matrix we get the following definition:

$$\sigma_\varepsilon(H) = \{z \in \mathbb{C} : \|(zI - H)^{-1}\| \geq \varepsilon^{-1}\}, \quad (\text{C2})$$

where $\|(zI - H)^{-1}\|$ is the resolvent of the matrix $zI - H$.

Finally, the so-called “poor man’s” pseudospectrum is the one we used for our main results. In a more rigorous way it is

$$\sigma_\varepsilon(H) = \{z \in \mathbb{C} : z \in \sigma(H + E) \text{ with } \|E\| \leq \varepsilon\}. \quad (\text{C3})$$

This is the only definition that accounts for structured perturbations.

The comparison between the different methods we mentioned above is shown in Fig. 7 for the three different lattices. Figures 7(a)–7(c) correspond to the infinite, finite, and interface lattice, respectively. As expected, all the definitions are equivalent. The cloud size of the interface lattice is larger than the other two (that are equal) due to the existence of an EP3 instead of an EP2.

Now we focus more on Eq. (C3). In particular, for the infinite and finite lattices we consider perturbations on the coupling coefficients, i.e., $E_{nm} = \delta_{n+1,m}z_n + \delta_{n,m+1}z_m^*$ (in order to preserve the \mathcal{PT} symmetry), diagonal perturbations with $E_{nm} = \delta_{n,m}z_n$, and a combination of the previous two. The reason is that a full pseudospectrum of the infinite lattice corresponds to a structured for the finite lattice. In more detail,

we have

$$E_c = \begin{bmatrix} 0 & z_1 & 0 & 0 & \cdots \\ z_1^* & 0 & z_2 & 0 & \cdots \\ 0 & z_2^* & 0 & z_1 & \cdots \\ 0 & 0 & z_1^* & 0 & \cdots \\ \vdots & \vdots & \vdots & \vdots & \ddots \end{bmatrix}, \quad (\text{C4})$$

where “c” stands for couplings and for diagonal (“d”) we have

$$E_d = \begin{bmatrix} z_1 & 0 & 0 & 0 & \cdots \\ 0 & z_2 & 0 & 0 & \cdots \\ 0 & 0 & z_3 & 0 & \cdots \\ 0 & 0 & 0 & z_4 & \cdots \\ \vdots & \vdots & \vdots & \vdots & \ddots \end{bmatrix} \quad (\text{C5})$$

We have to note here that our results for perturbations on the couplings are the same even when we do not preserve the \mathcal{PT} symmetry.

For the case of the interface lattice we perturb the diagonal the same way as above, while the coupling constants are as follows:

$$E_c^{\text{int}} = \begin{bmatrix} 0 & z_1 & 0 & 0 & \cdots \\ z_1 & 0 & z_2 & 0 & \cdots \\ 0 & z_2 & 0 & z_1 & \cdots \\ 0 & 0 & z_1 & 0 & \cdots \\ \vdots & \vdots & \vdots & \vdots & \ddots \end{bmatrix}. \quad (\text{C6})$$

Until now we have seen results for random perturbations on the diagonal that do not respect any symmetry. However, one might ask what happens if they do. Since our system is \mathcal{PT} symmetric we also demand the added diagonal perturbations to be \mathcal{PT} symmetric. In this case the perturbed matrix takes

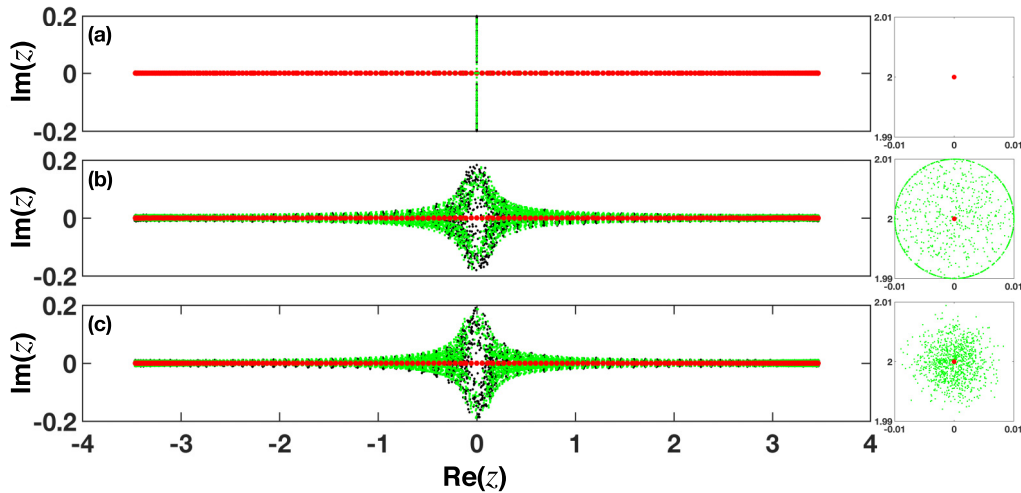


FIG. 8. Structured pseudospectra $\sigma_{0,01}^{\text{str}}(H)$, $s = 60$ of infinite (black dots) and finite (green dots, $N = 200$, $\gamma = 2$) NHSSH lattices. Red dots represent the conventional spectra. (a)–(c) correspond to off-diagonal (on coupling constants), on-diagonal, and combined perturbations, respectively. For each type of perturbations one of the edge states of the finite lattice is shown in the right column with $s = 1000$ realizations.

the form

$$E_d^{\mathcal{PT}} = \begin{bmatrix} z_1 & 0 & 0 & \dots & \dots & \dots & \dots & \dots & 0 \\ 0 & z_2 & 0 & \dots & \dots & \dots & \dots & \dots & 0 \\ \vdots & \vdots & \ddots & \dots & \dots & \dots & \dots & \dots & \vdots \\ 0 & \dots & \dots & z_{(N-1)/2} & \dots & \dots & \dots & \dots & 0 \\ 0 & \dots & \dots & \dots & \alpha_{(N-1)/2+1} & \dots & \dots & \dots & 0 \\ 0 & \dots & \dots & \dots & \dots & z_{(N-1)/2}^* & \dots & \dots & 0 \\ \vdots & \vdots & \vdots & \vdots & \vdots & \vdots & \ddots & \dots & \vdots \\ 0 & \dots & \dots & \dots & \dots & \dots & \dots & z_2^* & 0 \\ 0 & \dots & \dots & \dots & \dots & \dots & \dots & \dots & z_1^* \end{bmatrix}, \tag{C7}$$

where the element $E_{(N-1)/2+1,(N-1)/2+1} = \alpha_{(N-1)/2+1}$ has to be a real number, which is drawn from the standard normal distribution as the complex numbers z_n .

APPENDIX D: STRUCTURED PSEUDOSPECTRUM OF INFINITE AND FINITE LATTICES

Let us now consider the infinite and finite NHSSH. In the main text, we showed the corresponding complex pseudospectrum in Figs. 1(a) and 1(b), respectively. Regarding the structured pseudospectrum, we have calculated three different types of $\sigma_{0,01}^{\text{str}}(H)$, which are shown in Fig. 8. In particular, Figs. 8(a)–8(c) correspond to coupling [Eq. (C4)], diagonal [Eq. (C5)] with only the first two diagonal elements random, and the rest ones as copies of these two, combined perturbations ($E_c + E_d$), respectively. In terms of the EP’s sensitivity, both approaches give us similar results, something that is expected [53] for symmetric matrices. The difference from the complex pseudospectra is that the structured perturbations on the couplings reveal the topological robustness of the edge states, as is evident from Fig. 8(a).

APPENDIX E: COMPLEX AND STRUCTURED PSEUDOSPECTRUM OF THE INTERFACE LATTICE

Now we focus more on the interface lattice and present some additional results. One of the advantages of the contour

pseudospectrum [Eq. (C1)] is its capability to estimate the sensitivity of many and different perturbation strengths. In Fig. 9 we plot the pseudospectrum of the interface lattice using this method. The perturbation matrix E is a random complex matrix with size $N \times N$, i.e., $E \in \mathbb{C}^{N \times N}$ and we are at the EP.

Computing the pseudospectral radius ρ_ε around the EP for all values of ε is straightforward. Our results are shown in Fig. 10. The inset depicts small values of perturbation strength ε . As we expect, for small values we get a third root behavior (blue line) while for higher values the dependence becomes linear (black line). Retrieving such a result with other techniques can be challenging and time-consuming.

Let us now focus on structured pseudospectra. First, we examine the case when we perturb only one lattice site. We choose the lattice site next to the defect one, which is one of the three that forms the third-order EP. For different values of real perturbations we study the dependence of the eigenvalues

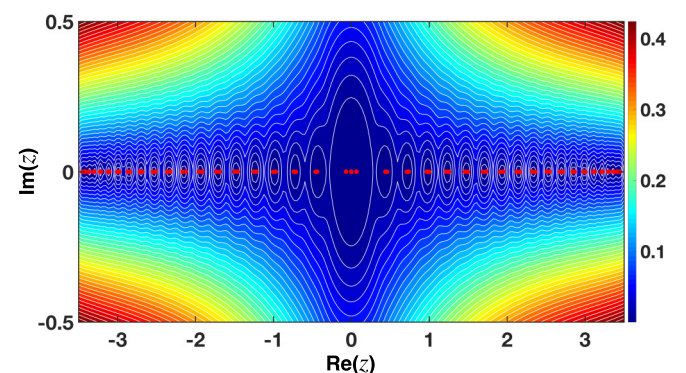


FIG. 9. The contour plot for different ε pseudospectra of the interface lattice in the complex plane for $\gamma = 2.015\,929\,3$. Red dots represent the eigenvalue spectrum of our unperturbed system. This is the full pseudospectrum of the whole spectrum using the SVD method we mentioned above. As expected, the sensitivity drops as we move away from the first gap.

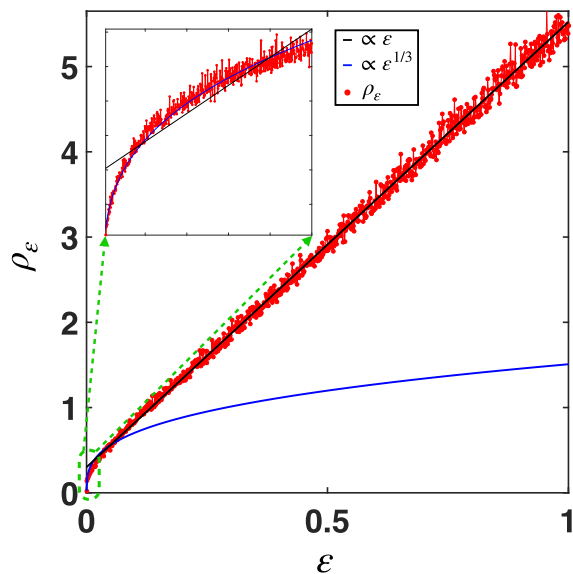


FIG. 10. Pseudospectral radius as a function of $\epsilon \in [10^{-6}, 1]$ for the interface lattice. The blue line is $\approx \epsilon^{1/3}$ and is shown for comparison while the black line is $\approx \epsilon$. The inset corresponds to values of $\epsilon \in [10^{-6}, 10^{-4}]$ where as we can see, we have excellent agreement with the third root behavior.

on them. The results are shown in Fig. 11, where the linear fit corresponds to a line with slope approximately 1/3. We expected this result since we have a third-order EP in our lattice.

Secondly, we present our results for diagonal \mathcal{PT} -symmetric perturbations using Eq. (C7). In this case we have

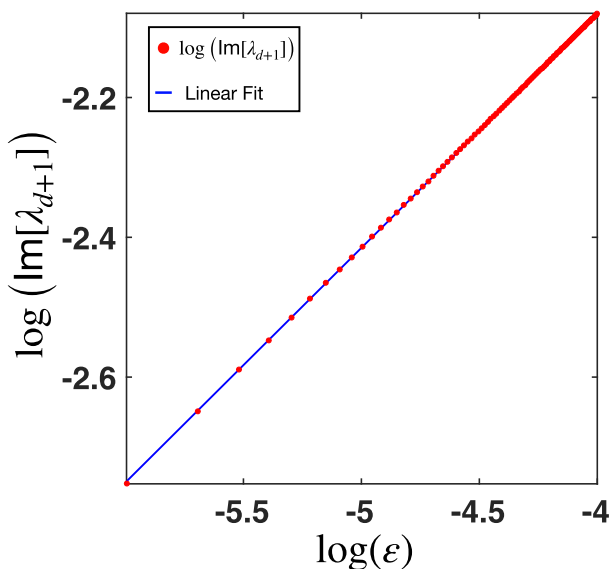


FIG. 11. Logarithmic plot of the dependence of the perturbed eigenvalue on the single site perturbation strength. Red dots correspond to the eigenvalues for different perturbations and the blue line is a linear fit. The slope is approximately 1/3 as expected for an EP3.

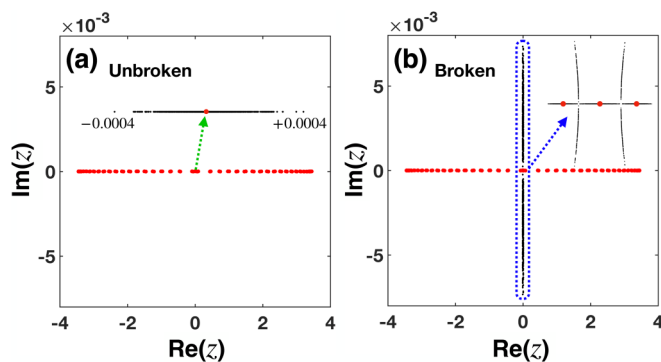


FIG. 12. Structured pseudospectra $\sigma_{10^{-6}}^{\text{str}}(H)$, $s = 1000$ of the interface NHSSH lattice for \mathcal{PT} -symmetric diagonal perturbations. (a) and (b) correspond to the unbroken ($\gamma = 2.015$) and broken ($\gamma = 2.0159$) regime, respectively. Insets depict the eigenvalue of the defect mode. As expected, it is perturbed only on the x axis (black dots) in the unbroken regime, while in the broken regime the eigenvalues become complex as seen for the three eigenvalues that form the EP3.

to examine two different regimes: the unbroken and the broken one. If we are close to the EP and the perturbations are small enough, then we are at the unbroken regime of the \mathcal{PT} symmetry. However, as we get closer to the EP and the band gap closes even more, such small perturbations can lead us to the broken regime. Our results are shown in Fig. 12. Figure 12(a) corresponds to the unbroken regime, while Fig. 12(b) corresponds to the broken one.

APPENDIX F: SPECTRAL BIFURCATION CURVES OF THE DETUNED INTERFACE LATTICE

One important aspect of the systems we consider, which was partially examined in the last part of the main text, is the possibility to create two extra lattices from the interface lattice. By tuning the gain-loss amplitude of the interface channel γ_0 , we can effectively induce two different lattices: a lossy lattice if the interface channel is lossy ($\gamma_0 > 0$, green),

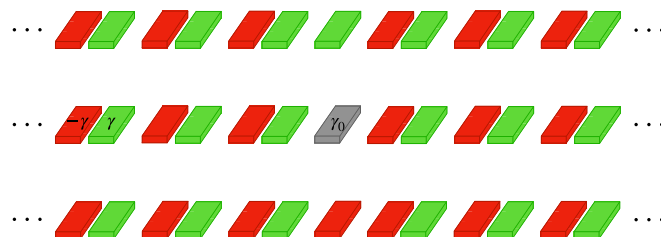


FIG. 13. Schematic illustration of three different interface lattices. Notice that the only difference is at the interface channel, which can be lossy (top), gainy (bottom), or neutral (middle). Only the middle system is \mathcal{PT} symmetric.

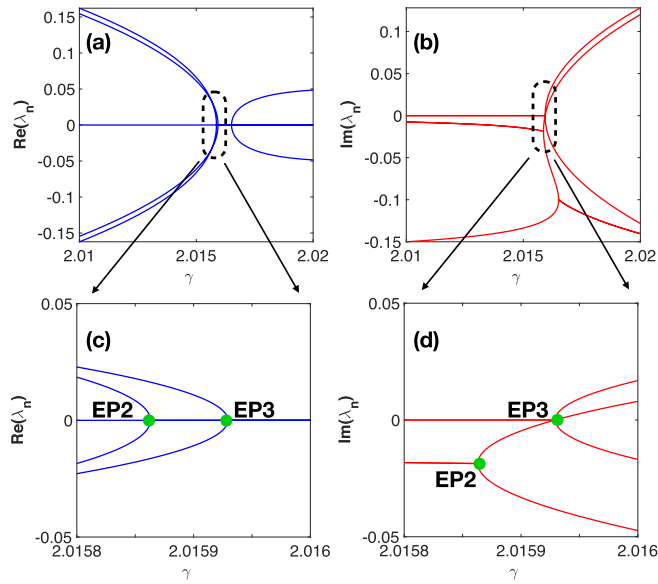


FIG. 14. Bifurcation diagram of the (a) Real part, (b) Imaginary part of the defect mode and its four neighboring modes vs the gain-loss amplitude for the gainy lattice ($\gamma_0 = -0.3$). (c) and (d) are magnified view of the dashed rectangular in (a) and (b) to clearly see the two different EPs that are formed. Green dots represent the EPs.

and a gainy lattice ($\gamma_0 < 0$, red) if the interface channel has gain, as shown in Fig. 13. These two different lattices are a complex conjugate pair and are not \mathcal{PT} symmetric.

The Hamiltonians of these three different lattices are related. If we denote as H_G the gainy Hamiltonian, H_L the lossy one, and finally H_N the neutral, the relation between them is trivially derived, i.e., $H_N = \frac{H_G + H_L}{2}$. If we act with the \mathcal{PT} operators on the Hamiltonians, then we get the relations $\hat{P}\hat{T}H_G = H_L$, $\hat{P}\hat{T}H_L = H_G$, and $\hat{P}\hat{T}H_N = H_N$. This is expected since only the middle lattice H_N is \mathcal{PT} symmetric as we mentioned before. Furthermore, the spectra of these three lattices are quite similar. The real part of the eigenvalues will be the same for the three lattices and only the imaginary part will be different, since the new lattices are complex conjugate.

The bifurcation curves of the gainy lattice are shown in Fig. 14. As we can see from Figs. 14(c) and 14(d), we first cross a second-order EP and then the third-order EP. However, the value for the third-order EP is still the same as it was for the \mathcal{PT} lattice, i.e., $\gamma = 2.0159293$. Depending on the value of γ_0 , the second-order EP is moving either away from the third order one or towards it. However, it never goes after the third-order EP. Despite these two EPs being very close to each other, we can still distinguish the eigenmodes that form them and their corresponding amplitudes.

- [1] N. Moiseyev, *Non-Hermitian Quantum Mechanics* (Cambridge University Press, New York, 2011).
- [2] M. V. Berry, Physics of nonhermitian degeneracies, *Czech. J. Phys.* **54**, 1039 (2004).
- [3] W. D. Heiss, Exceptional points of non-Hermitian operators, *J. Phys. A: Math. Gen.* **37**, 2455 (2004).
- [4] J. Wiersig, S.-W. Kim, and M. Hentschel, Asymmetric scattering and nonorthogonal mode patterns in optical microspirals, *Phys. Rev. A* **78**, 053809 (2008).
- [5] S. B. Lee, J. Yang, S. Moon, S. Y. Lee, J. B. Shim, S. W. Kim, J. H. Lee, and K. An, Observation of an Exceptional Point in a Chaotic Optical Microcavity, *Phys. Rev. Lett.* **103**, 134101 (2009).
- [6] C. M. Bender and S. Boettcher, Real Spectra in Non-Hermitian Hamiltonians Having \mathcal{PT} Symmetry, *Phys. Rev. Lett.* **80**, 5243 (1998).
- [7] C. M. Bender, S. Boettcher, and P. N. Meisinger, \mathcal{PT} -symmetric quantum mechanics, *J. Math. Phys.* **40**, 2201 (1999).
- [8] C. M. Bender, D. C. Brody, and H. F. Jones, Complex Extension of Quantum Mechanics, *Phys. Rev. Lett.* **89**, 270401 (2002).
- [9] R. El-Ganainy, K. G. Makris, D. N. Christodoulides, and Z. H. Musslimani, Theory of coupled optical \mathcal{PT} -symmetric structures, *Opt. Lett.* **32**, 2632 (2007).
- [10] K. G. Makris, R. El-Ganainy, D. N. Christodoulides, and Z. H. Musslimani, Beam Dynamics in \mathcal{PT} Symmetric Optical Lattices, *Phys. Rev. Lett.* **100**, 103904 (2008).
- [11] Z. H. Musslimani, K. G. Makris, R. El-Ganainy, and D. N. Christodoulides, Optical Solitons in \mathcal{PT} Periodic Potentials, *Phys. Rev. Lett.* **100**, 030402 (2008).
- [12] A. Guo, G. J. Salamo, D. Duchesne, R. Morandotti, M. Volatier-Ravat, V. Aimez, G. A. Siviloglou, and D. N. Christodoulides, Observation of \mathcal{PT} -Symmetry Breaking in Complex Optical Potentials, *Phys. Rev. Lett.* **103**, 093902 (2009).
- [13] C. E. Rüter, K. G. Makris, R. El-Ganainy, D. N. Christodoulides, M. Segev, and D. Kip, Observation of parity-time symmetry in optics, *Nat. Phys.* **6**, 192 (2010).
- [14] Y. D. Chong, L. Ge, and A. D. Stone, \mathcal{PT} -Symmetry Breaking and Laser-Absorber Modes in Optical Scattering Systems, *Phys. Rev. Lett.* **106**, 093902 (2011).
- [15] L. Ge, Y. D. Chong, and A. D. Stone, Conservation relations and anisotropic transmission resonances in one-dimensional \mathcal{PT} -symmetric photonic heterostructures, *Phys. Rev. A* **85**, 023802 (2012).
- [16] P. Ambichl, K. G. Makris, L. Ge, Y. D. Chong, A. D. Stone, and S. Rotter, Breaking of \mathcal{PT} Symmetry in Bounded and Unbounded Scattering Systems, *Phys. Rev. X* **3**, 041030 (2013).
- [17] A. Regensburger, C. Bersch, M.-A. Miri, G. Onishchukov, D. N. Christodoulides, and U. Peschel, Parity-time synthetic photonic lattices, *Nature (London)* **488**, 167 (2012).
- [18] L. Feng, Y.-L. Xu, W. S. Fegadolli, M.-H. Lu, J. E. B. Oliveira, V. R. Almeida, Y.-F. Chen, and A. Scherer, Experimental demonstration of a unidirectional reflectionless parity-time metamaterial at optical frequencies, *Nat. Mater.* **12**, 108 (2013).
- [19] B. Peng, S. K. Ozdemir, F. Lei, F. Monifi, M. Gianfreda, G. L. Long, S. Fan, F. Nori, C. M. Bender, and L. Yang, Parity-time-symmetric whispering-gallery microcavities, *Nat. Phys.* **10**, 394 (2014).
- [20] L. Feng, Z. Jing Wong, R.-M. Ma, Y. Wang, and X. Zhang, Single-mode laser by parity-time symmetry breaking, *Science* **346**, 972 (2014).

- [21] H. Hodaei, M.-A. Miri, M. Heinrich, D. N. Christodoulides, and M. Khajavikhan, Parity-time-symmetric microring lasers, *Science* **346**, 975 (2014).
- [22] B. Peng, S. K. Özdemir, S. Rotter, H. Yilmaz, M. Liertzer, F. Monifi, C. M. Bender, F. Nori, and L. Yang, Loss-induced suppression and revival of lasing, *Science* **346**, 328 (2014).
- [23] S. Assaworrorarit, X. Yu, and S. Fan, Robust wireless power transfer using a nonlinear parity-time-symmetric circuit, *Nature (London)* **546**, 387 (2017).
- [24] J. Zhang, B. Peng, S. K. Özdemir, K. Pichler, D. O. Krimer, G. Zhao, F. Nori, Y. Liu, S. Rotter, and L. Yang, A phonon laser operating at an exceptional point, *Nat. Photon.* **12**, 479 (2018).
- [25] H. Hodaei, A. U. Hassan, S. Wittek, H. Garcia-Gracia, R. El-Ganainy, D. N. Christodoulides, and M. Khajavikhan, Enhanced sensitivity at higher-order exceptional points, *Nature (London)* **548**, 187 (2017).
- [26] M. P. Hokmabadi, A. Schumer, D. N. Christodoulides, and M. Khajavikhan, Non-Hermitian ring laser gyroscopes with enhanced Sagnac sensitivity, *Nature (London)* **576**, 70 (2019).
- [27] T. Kottos, Broken symmetry makes light work, *Nat. Phys.* **6**, 166 (2010).
- [28] D. F. Pile and D. N. Christodoulides, Gaining with loss, *Nat. Photon.* **11**, 742 (2017).
- [29] R. El-Ganainy, K. G. Makris, M. Khajavikhan, Z. H. Musslimani, S. Rotter, and D. N. Christodoulides, Non-Hermitian physics and \mathcal{PT} symmetry, *Nat. Phys.* **14**, 11 (2018).
- [30] S. K. Özdemir, S. Rotter, F. Nori, and L. Yang, Parity-time symmetry and exceptional points in photonics, *Nat. Mater.* **18**, 783 (2019).
- [31] M. A. Miri and A. Alu, Exceptional points in optics and photonics, *Science* **363**, eaar7709 (2019).
- [32] N. Malkova, I. Hromada, X. Wang, G. Bryant, and Z. Chen, Observation of optical Shockley-like surface states in photonic superlattices, *Opt. Lett.* **34**, 1633 (2009).
- [33] Z. Wang, Y. Chong, J. D. Joannopoulos, and M. Soljacic, Observation of unidirectional backscattering-immune topological electromagnetic states, *Nature (London)* **461**, 772 (2009).
- [34] M. C. Rechtsman, J. M. Zeuner, Y. Plotnik, Y. Lumer, D. Podolsky, F. Dreisow, S. Nolte, M. Segev, and A. Szameit, Photonic Floquet topological insulators, *Nature (London)* **496**, 196 (2013).
- [35] M. A. Bandres, M. C. Rechtsman, and M. Segev, Topological Photonic Quasicrystals: Fractal Topological Spectrum and Protected Transport, *Phys. Rev. X* **6**, 011016 (2016).
- [36] A. Blanco-Redondo, B. Bell, D. Oren, B. J. Eggleton, and M. Segev, Topological protection of biphoton states, *Science* **362**, 568 (2018).
- [37] S. Mukherjee and M. C. Rechtsman, Observation of Floquet solitons in a topological bandgap, *Science* **368**, 856 (2020).
- [38] S. Xia *et al.*, Nontrivial coupling of light into a defect: The interplay of nonlinearity and topology, *Light Sci. Appl.* **9**, 147 (2020).
- [39] M. Parto, S. Wittek, H. Hodaei, G. Harari, M. A. Bandres, J. Ren, M. C. Rechtsman, M. Segev, D. N. Christodoulides, and M. Khajavikhan, Edge-Mode Lasing in 1D Topological Active Arrays, *Phys. Rev. Lett.* **120**, 113901 (2018).
- [40] G. Harari, M. Bandres, Y. Lumer, M. Rechtsman, Y. Chong, M. Khajavikhan, D. N. Christodoulides, and M. Segev, Topological insulator laser: Theory, *Science* **359**, eaar4003 (2018).
- [41] M. Bandres, S. Wittek, G. Harari, M. Parto, J. Ren, M. Segev, D. N. Christodoulides, and M. Khajavikhan, Topological insulator laser: Experiments, *Science* **359**, eaar4005 (2018).
- [42] H. Zhao, X. Qiao, T. Wu, B. Midya, S. Longhi, and L. Feng, Non-Hermitian topological light steering, *Science* **365**, 1163 (2019).
- [43] Y. G. N. Liu, P. S. Jung, M. Parto, D. N. Christodoulides, and M. Khajavikhan, Gain-induced topological response via tailored long-range interactions, *Nat. Phys.* **17**, 704 (2021).
- [44] W. P. Su, J. R. Schrieffer, and A. J. Heeger, Solitons in Polyacetylene, *Phys. Rev. Lett.* **42**, 1698 (1979).
- [45] S. Weimann, M. Kremer, Y. Plotnik, Y. Lumer, S. Nolte, K. G. Makris, M. Segev, M. Rechtsman, and A. Szameit, Topologically protected bound states in photonic parity-time-symmetric crystals, *Nat. Mater.* **16**, 433 (2017).
- [46] S. Xia, D. Kaltsas, D. Song, I. Komis, J. Xu, A. Szameit, H. Buljan, K. G. Makris, and Z. Chen, Nonlinear tuning of \mathcal{PT} symmetry and non-Hermitian topological states, *Science* **372**, 72 (2021).
- [47] Z. Gong, Y. Ashida, K. Kawabata, K. Takasan, S. Higashikawa, and M. Ueda, Topological Phases of Non-Hermitian Systems, *Phys. Rev. X* **8**, 031079 (2018).
- [48] K. Kawabata, K. Shiozaki, M. Ueda, and M. Sato, Symmetry and Topology in Non-Hermitian Physics, *Phys. Rev. X* **9**, 041015 (2019).
- [49] K. Takata and M. Notomi, Photonic Topological Insulating Phase Induced Solely by Gain and Loss, *Phys. Rev. Lett.* **121**, 213902 (2018).
- [50] X. W. Luo and C. Zhang, Higher-Order Topological Corner States Induced by Gain and Loss, *Phys. Rev. Lett.* **123**, 073601 (2019).
- [51] S. Longhi, Topological Phase Transition in Non-Hermitian Quasicrystals, *Phys. Rev. Lett.* **122**, 237601 (2019).
- [52] S. Sayyad and F. K. Kunst, Realizing exceptional points of any order in the presence of symmetry, *Phys. Rev. Res.* **4**, 023130 (2022).
- [53] L. N. Trefethen and M. Embree, *Spectra and Pseudospectra* (Princeton University Press, Princeton, NJ, 2005).
- [54] L. N. Trefethen, A. E. Trefethen, S. C. Reddy, and T. A. Driscoll, Hydrodynamic stability without eigenvalues, *Science* **261**, 578 (1993).
- [55] L. N. Trefethen, Pseudospectra of linear operators, *SIAM Rev.* **39**, 383 (1997).
- [56] L. N. Trefethen, Computation of pseudospectra, *Acta Numer.* **8**, 247 (1999).
- [57] N. Hatano and D. R. Nelson, Localization Transitions in Non-Hermitian Quantum Mechanics, *Phys. Rev. Lett.* **77**, 570 (1996).
- [58] G. Baggio *et al.*, Efficient communication over complex dynamical networks: The role of matrix non-normality, *Sci. Adv.* **6**, eaba2282 (2020).
- [59] S. C. Reddy, P. J. Schmid, and D. S. Henningson, Pseudospectra of the Orr-Sommerfeld Operator, *SIAM J. Appl. Math.* **53**, 15 (1993).
- [60] S. C. Reddy and D. S. Henningson, Energy growth in viscous channel flows, *J. Fluid Mech.* **252**, 209 (1993).
- [61] J. S. Baggett, T. A. Driscoll, and L. N. Trefethen, A mostly linear model of transition to turbulence, *Phys. Fluids* **7**, 833 (1995).

- [62] P. J. Schmid, Linear stability theory and bypass transition in shear flows, *Phys. Plasmas* **7**, 1788 (2000).
- [63] K. G. Makris, L. Ge, and H. E. Türeci, Anomalous Transient Amplification of Waves in Non-normal Photonic Media, *Phys. Rev. X* **4**, 041044 (2014).
- [64] K. G. Makris, Transient growth and dissipative exceptional points, *Phys. Rev. E* **104**, 054218 (2021).
- [65] S. Longhi and P. Laporta, Excess noise in intracavity laser frequency modulation, *Phys. Rev. E* **61**, R989 (2000).
- [66] F. Papoff, G. D'Alessandro, and G. L. Oppo, State Dependent Pseudoresonances and Excess Noise, *Phys. Rev. Lett.* **100**, 123905 (2008).
- [67] N. Okuma and M. Sato, Hermitian zero modes protected by nonnormality: Application of pseudospectra, *Phys. Rev. B* **102**, 014203 (2020).
- [68] N. Okuma and M. Sato, Non-Hermitian Skin Effects in Hermitian Correlated or Disordered Systems: Quantities Sensitive or Insensitive to Boundary Effects and Pseudo-Quantum-Number, *Phys. Rev. Lett.* **126**, 176601 (2021).
- [69] Y. Ashida, Z. Gong, and M. Ueda, Non-Hermitian physics, *Adv. Phys.* **69**, 249 (2020).
- [70] E. B. Davies and M. Hager, Perturbations of Jordan matrices, *J. Approx. Theory* **156**, 82 (2009).